Journal of Applied Polymer Science

WILEY

Applied Polymer SCIENCE

RESEARCH ARTICLE OPEN ACCESS

Flexible Dry Electrodes Based on Styrene-Ethylene-Butylene-Styrene/Carbon Black and Ethylene-Vinyl Acetate/Carbon Black for Electroencephalography: Electrical, Thermal and Mechanical Properties

George Gnonhoue | Ilyass Tabiai | Jérémie Voix | Éric David

Université du Québec, École de technologie supérieure, Montreal, Canada

Correspondence: George Gnonhoue (olatoundji-george.gnonhoue.1@ens.etsmtl.ca)

Received: 15 August 2025 | **Revised:** 19 November 2025 | **Accepted:** 30 November 2025

Keywords: biomedical applications | copolymers | dielectric properties | mechanical properties | sensors and actuators

ABSTRACT

Electroencephalography (EEG) is an essential technique for monitoring brain electrical activity in clinical, sports, and wearable health settings. However, traditional wet electrodes face issues like gel drying and skin irritation, while coated dry electrodes tend to degrade over time, affecting long-term signal stability. This study explores flexible dry electrodes made from conductive polymer composites—poly(styrene-b-ethylene-ran-butylene-b-styrene) filled with carbon black (SEBS/CB) and ethylene-vinyl acetate filled with carbon black (EVA/CB)—as affordable and recyclable alternatives to standard materials such as PDMS and TPU. The electrodes were manufactured using solvent casting and compression molding, ensuring even filler distribution and consistent surface quality. Both composites reached an electrical conductivity of around 0.01 S/m with a percolation threshold close to 12 wt% CB. Contact impedance tests showed better performance for SEBS/CB electrodes (5.4 ± 0.9 kΩ) compared to EVA/CB (26.7 ± 4.4 kΩ), nearing the value of a commercial flexible electrode (4.2 ± 0.5 kΩ). Mechanical testing confirmed that SEBS/CB is softer and more elastic, facilitating stable, low-noise EEG signal collection. Overall, SEBS/CB composites provide a good balance of electrical performance, flexibility, and scalability, highlighting their potential for next-generation, long-term EEG monitoring systems.

1 | Introduction

Electroencephalography (EEG) measures brain electrical activity via scalp electrodes, reflecting physiological and cognitive states [1–4]. EEG signals, classified into Delta (0.5–4 Hz), Theta (4–8 Hz), Alpha (8–12 Hz), Beta (12–30 Hz), and Gamma (30+ Hz) bands, are fundamental for diagnosing neurological disorders and for continuous brain–computer interface (BCI) and health monitoring applications. The reliability of EEG recordings strongly depends on maintaining low skin–electrode contact impedance, which ensures a stable signal-to-noise ratio and accurate measurements [5–7]. Traditional wet electrodes, despite their low impedance and high signal quality, have notable drawbacks such as gel drying, skin irritation, and instability during extended use or movement [1–3, 8–15]. As a result, research has shifted toward dry flexible electrodes, which eliminate the need for electrolytic gels and are better suited for wearable and long-term applications. These gel-free electrodes

need materials that are flexible, biocompatible, and electrically conductive to ensure signal quality under different mechanical deformations [16, 17].

Flexible polymers are commonly used as base materials, with material choices varying based on design, application, and user needs in clinical, research, or consumer settings. Dry flexible electrodes enhance comfort during long-term EEG by conforming to the scalp's curvatures, maintaining stable contact even during movement, and improving signal quality. While these electrodes present a higher impedance than wet ones, optimizing the surface texture and design can minimize contact impedance, enhance skin contact, and reduce motion artifacts. Effective designs, such as those using silver-coated electrodes [7, 18], ensure stable signals, comfort, and minimal irritation. These electrodes achieve impedance levels below 50 kΩ at 10 Hz, making them suitable for reliable and prolonged EEG recordings [19, 20].

Over the past few years, various materials have been investigated to achieve this balance. PDMS (polydimethylsiloxane) and TPU (thermoplastic polyurethane) have been widely used due to their softness and skin compatibility, but their relatively high contact impedance and limited recyclability constrain their performance and scalability (TPU) [21–26]. For instance, Fiedler et al. [6] developed Ag/AgCl-coated polyurethane electrodes that reached ~150 kΩ impedance, while Heijs et al. [27] reported 602 ± 401 kΩ using similar multipin electrodes. Recent efforts have explored conductive coatings and composite formulations—such as silver-filled TPU [28], carbon black (CB)/TPU [29], graphene/PDMS composites [5], and multi-walled carbon nanotube (MWCNT)–PDMS mixtures [30, 31], achieving moderate improvements in flexibility and signal quality. Nevertheless, contact impedance typically remains in the 10–600 kΩ range, which is still considerably higher than that of wet electrodes.

To overcome these challenges, attention has increasingly turned toward thermoplastic elastomers (TPEs) that combine the softness of rubbers with the processability of plastics. Among them, Styrene-Ethylene-Butylene-Styrene (SEBS) and Ethylene-Vinyl Acetate (EVA) have emerged as promising alternatives. SEBS exhibits exceptional elasticity, softness, and chemical resistance, making it ideal for skin-interfacing biomedical devices. EVA offers comparable flexibility, biocompatibility, and easy processing, with adjustable mechanical properties depending on its vinyl acetate content [32]. Both materials are recyclable thermoplastics, contrasting with non-recyclable PDMS, and they are compatible with scalable manufacturing processes such as extrusion, injection molding, and 3D printing—key advantages for the mass production of wearable biosensors [33, 34].

When combined with conductive fillers such as carbon black (CB), carbon fibers, or graphene, these matrices can form lightweight, low-cost conductive composites suitable for EEG electrodes. CB is particularly advantageous due to its high surface area, ease of dispersion, chemical stability, and significantly lower cost than CNTs or graphene. Recent works [35, 36] have shown that SEBS- and EVA-based composites exhibit tunable conductivity and mechanical properties, making them strong candidates for flexible bioelectronic applications. However, their use in EEG electrodes has not yet been thoroughly explored or benchmarked against established PDMS- and TPU-based designs, leaving a clear gap in the literature.

The present study addresses this gap by systematically investigating SEBS/CB and EVA/CB composites as alternative materials for flexible dry EEG electrodes. Using a chemical dissolution method for homogeneous filler dispersion, flexible electrodes were fabricated and characterized for their electrical conductivity, contact impedance, mechanical compliance, and EEG signal acquisition capability. The obtained results were directly compared with those of commercial dry electrodes and benchmarked against recent PDMS- and TPU-based designs from the literature.

This work highlights, for the first time, the comparative advantages of SEBS- and EVA-based carbon black composites in balancing low contact impedance, high flexibility, and scalable manufacturability. Beyond performance improvement, the use of thermoplastic matrices introduces sustainability and cost-efficiency benefits that are critical for the next generation of wearable EEG systems. The study thus contributes to expanding the material platform for bioelectronic interfaces by proposing recyclable, high-performance elastomeric composites for durable and comfortable long-term EEG applications. Section 1 outlines the methodology for developing and characterizing SEBS/CB and EVA/CB electrodes, focusing on the surface morphology, compression testing, electrical properties, contact impedance, and brain signal acquisition. Results are compared with those of commercial dry flexible EEG electrodes. Section 2 details the experimental procedures used to prepare and characterize SEBS/CB and EVA/CB electrodes, including composite formulation, electrode fabrication, morphological analysis, mechanical testing, electrical characterization, and EEG signal acquisition methodology. The discussion addresses the study's limitations and suggests directions for future research. The objective is to determine the composite material that offers the optimal combination of electrical conductivity, low contact impedance, mechanical compliance, thermal stability, and scalp conformity. This work ultimately seeks to advance the development of durable, high-performance EEG electrodes designed for long-term, real-world applications.

2 | Experimental Testing

This section details the materials, preparation methods, and fabrication process used to develop SEBS/CB and EVA/CB flexible EEG electrodes. The main aim is to compare the performance of SEBS/CB and EVA/CB materials with that of a commercial dry flexible electrode to identify which provides superior electrical conductivity and lower contact impedance for recording brain electrical signals. The methodology was designed to ensure reproducibility and facilitate other researchers in replicating the fabrication process. All experimental procedures were conducted under controlled conditions, with the purity and specifications of the materials used clearly outlined. A future clinical study involving long-term, multi-participant EEG recordings is planned.

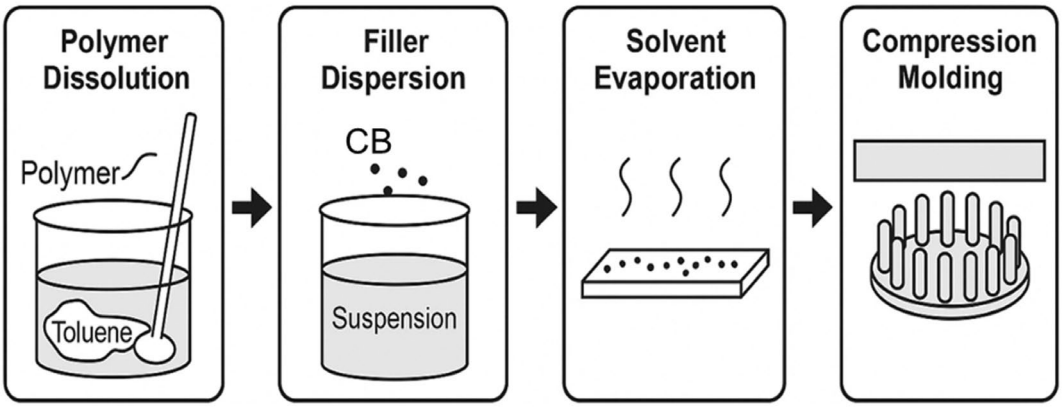

FIGURE 1 | Schematic overview of the fabrication process for flexible multipin dry electrodes. The method includes (i) dissolving the SEBS or EVA polymer in toluene, (ii) dispersing conductive fillers (CB) to create a uniform suspension, (iii) evaporating the solvent to form composite films, and (iv) using compression molding to shape the films into multipin electrode structures.

TABLE 1 | SEBS/CB and EVA/CB nanocomposites at different carbon nanoparticle weight fractions.

SEBS/CB (wt%)		EVA/CB (wt%)	
Reinforcements	**Matrix**	**Reinforcements**	**Matrix**
0	100	0	100
3	97	5	95
5	95	8	92
6	94	12	88
7	93	16.5	83.5
8	92	18.5	81.5
10	90	20	80
12	88		
15	85		
20	80		

2.1 | Materials

Two thermoplastic matrices were selected: Styrene–ethylene–butylene–styrene (SEBS) and ethylene–vinyl acetate (EVA), chosen for their elasticity and mechanical resilience.

- SEBS, with a number-average molecular weight of 54,000 g/mol and a polystyrene content of 30 wt%, was supplied by Kraton Polymers (Paulínia, Brazil) with a purity greater than 99%.
- EVA (vinyl acetate content 28 wt%, density 0.950 g/cm^3) was obtained from Repsol (Madrid, Spain), analytical grade, with a purity of over 98%.
- Carbon black nanoparticles (Carbon Lampblack C198-500, Lot 145,509, average diameter approximately 50 nm, nominal conductivity around 400 S/m, density = 1.8 g/cm^3) were sourced from Fisher Chemical (Ottawa, Canada), with a purity over 99%.
- Toluene (UN1294, Optima grade, Lot 234,238) was used as a solvent and obtained from Fisher Chemical (Ottawa, Canada), with a purity of ≥ 99.8%.

All materials were used as received without further purification. The preparation steps were carried out in a fume hood to ensure solvent safety and process safety repeatability.

2.2 | Preparation of SEBS/CB and EVA/CB Composites

The preparation process involved four main stages: dissolving the polymer, dispersing the filler, and removing the solvent, as shown schematically in Figure 1.

2.2.1 | Polymer Dissolution

Each polymer (SEBS or EVA) was dissolved separately in toluene at 100°C with magnetic stirring (600 rpm) until a clear, homogeneous solution was achieved.

2.2.2 | Filler Incorporation

After complete dissolution, carbon black (CB) was gradually added to the polymer solution at various mass fractions ranging from 0 to 20 wt% (see Table 1). The mixture was stirred for an extra 30 min at 100°C to ensure uniform dispersion of CB within the matrix. The formation of the composite depended on the physical entanglement of polymer chains with the conductive CB network, enabling efficient electron transport after the solvent was removed.

SEBS, owing to its elastomeric block-copolymer architecture, accommodates higher filler loadings because of its greater chain mobility and tolerance to viscosity increases. In contrast, EVA exhibits a marked rise in viscosity at elevated CB contents, which restricts its processability under identical mixing and molding conditions.

2.2.3 | Solvent Evaporation and Film Formation

The resulting dispersions were cast and left to dry under a chemical fume hood at room temperature until all solvent evaporated, resulting in nanocomposite films.

2.3 | Fabrication of Surface Multipin EEG Electrodes

The solid composites were molded into surface multipin EEG electrodes using compression molding (Figure 1).

- Step 1: Pre-heating and low-pressure molding at 215°C, 0.8 MPa, 5 min.
- Step 2: High-pressure consolidation at 215°C, 5 MPa, 15 min.

Each electrode consisted of 19 cylindrical pins arranged in a circular pattern. The pins had an average height of 4.9 ± 0.09 mm and a diameter of 1.41 ± 0.01 mm. The center-to-center distance between neighboring pins was about 2.5 mm, which corresponds to an edge-to-edge spacing of approximately 1.1 mm at the electrode–skin interface.

2.4 | Optimization and Reproducibility

Distinct CB loadings were explored for SEBS and EVA to identify the electrical percolation threshold and the conductivity plateau for each matrix. For both material systems, the composite exhibiting the highest electrical conductivity was selected for subsequent electrical, mechanical, and morphological characterizations. To ensure reproducibility, three independent batches of each selected formulation were fabricated and characterized under identical conditions.

2.5 | Characterizations

2.5.1 | Electrical Characterization

The electrical conductivities of the different composites were not measured using conventional electrophysiological techniques (e.g., impedance at fixed frequencies or skin-contact methods), but rather using a frequency-domain dielectric spectrometer (Alpha-A Dielectric Analyzer, BDS—Novocontrol, Montabaur, Germany) to characterize their intrinsic bulk conductivity. For each formulation, measurements were performed on three independent samples to ensure reproducibility. Each sample was shaped into a 20 mm-diameter and 1.2 mm-thick disk and placed between two solid brass electrodes to form a planar electrode/composite/electrode sandwich. This setup allows for accurate determination of the real part of the complex conductivity over a wide frequency range (10^{-2} to 10^{5} Hz) at 30°C. The aim was to assess percolation behavior and frequency dependence of conductivity in the bulk material, independently of contact with biological tissue.

2.5.2 | Structural Characterization

To study the distribution of the conductive particles in the host matrix, the morphology of the composites was investigated using a high-resolution scanning electron microscope (Hitachi SU-8230 field emission-SEM) at 5 kV. Cross-sections of the specimens were prepared using a cryogenic fracture technique, after which they were coated with a platinum layer of approximately 2 nm under vacuum conditions using a turbo-pumped sputter coater/carbon coater (Q150T).

2.5.3 | Thermal Characterization

Differential Scanning Calorimetry (DSC) was employed to investigate the thermal properties of the pure polymer matrices (SEBS and SEBS-MA). Tests were conducted in a nitrogen atmosphere to prevent oxidation. Approximately 10 mg samples were sealed in aluminum pans and heated at a rate of 10°C/min. To avoid thermal degradation, the measurement ranges were tailored to the thermal stability of each material: −100°C–250°C. These conditions facilitated the detection of key transitions, including the glass transitions of both the soft and hard phases, without interference from decomposition.

2.5.4 | Mechanical Characterization

Cyclic compression tests were conducted on SEBS/20 wt% CB and EVA/20 wt% CB composites using the ASTM D575-91 standard to define specimen geometry and test conditions. Standard cylindrical specimens measured 28.6 ± 0.1 mm in diameter and 12.5 ± 0.5 mm in thickness. A compressive load of 100 kN was applied using a universal testing machine (MTS Alliance RF/200, MTS Systems Corporation, Eden Prairie, Minnesota, United States). Each test involved three consecutive loading–unloading cycles to evaluate the flexibility, shape memory behavior, and mechanical repeatability of the materials. All measurements were carried out under ambient laboratory conditions, with a temperature of approximately 23°C and relative humidity of 45%–55%.

To characterize the mechanical performance, key parameters were extracted from the stress–strain curves, including the stress at 50% compression, the elastic modulus, the hysteresis loss (energy dissipated per cycle), the loading energy, and the energy ratios between cycles to assess energy retention and mechanical stability. Tests were performed on three independent samples per material to ensure repeatability and statistical reliability of the results.

2.6 | Experimental Validation in Vivo

Multipin flexible EEG electrodes were selected to evaluate contact impedance and EEG artifacts associated with eye movements. These artifacts were wirelessly recorded using the OpenBCI 16-channel Cyton Biosensing Board (OpenBCI, NY, USA) in combination with the Ultracortex 'Mark IV' EEG headset (OpenBCI, NY, USA). Contact impedance was measured at 31 Hz using the same acquisition system, as shown in Figure 2.

To simulate practical conditions for wearable EEG applications, the skin was neither cleaned nor abraded before measurements. The headset, in which the electrodes were inserted, was

comfortably positioned on the head without applying pressure to the electrode surfaces. A commercial dry flexible electrode (OpenBCI, NY, USA) was placed at position 2 (see Figure 2), while the multipin electrodes developed in this study were inserted at positions 1 and 3.

Figure 3 shows the custom-designed multipin electrode alongside the commercial flexible electrode used as a reference. Performance evaluation was based on comparisons of contact impedance and EEG signal amplitude between the developed and commercial electrodes. The measurement system consisted of a ground, a reference electrode, and the developed electrode, allowing impedance to be measured between the developed and reference electrodes. Figure 2 illustrates the Ultracortex 'Mark IV' EEG headset used for signal acquisition and impedance measurements.

2.7 | Participants

Participant testing validated the effectiveness of the developed electroencephalogram (EEG) electrodes under physiological conditions by assessing EEG signal quality and motion artifacts. Healthy adult participants ($n = 4$; 1 male and 3 females, aged between 21 and 35 years) were recruited for EEG measurements.

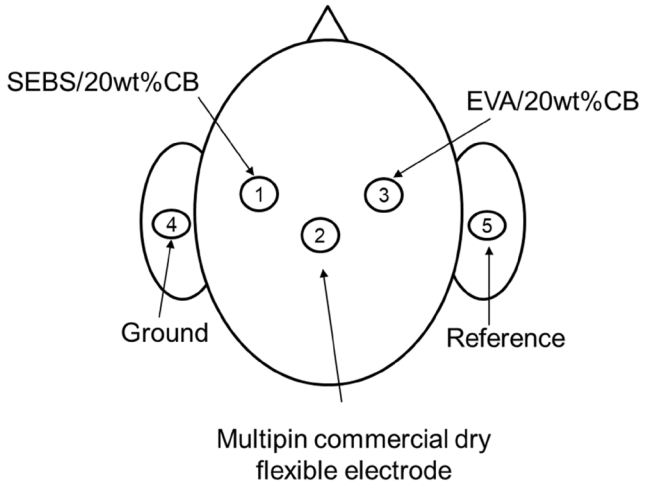

FIGURE 2 | Ultracortex "Mark IV" EEG headset used to install the electrodes on the head.

All procedures were approved by the ÉTS Internal Review Board (« Comité d'éthique de la recherche », Approval No. H20230504) and conducted in accordance with the Declaration of Helsinki. Informed consent was obtained from all participants before the experiments.

To ensure a controlled environment, participants were comfortably seated in a quiet room during signal acquisition. EEG signals were recorded for 10 s. Following standard EEG protocols and the American Clinical Neurophysiology Society guidelines [37], participants were instructed to minimize head and facial muscle movements and remain still to reduce motion artifacts. At designated time points—approximately at 1, 3, 8, and 10 s—they were asked to blink in response to a sound cue to evaluate the electrodes' ability to detect blink-related EEG activity.

3 | Results

3.1 | Electrical, Structural and Mechanical Properties

3.1.1 | Electrical Properties

Figure 4 depicts the frequency dependence of the real part of the complex conductivity (σ') for SEBS and EVA composites with various carbon black loadings. Only the real part is shown here, as it directly reflects the conductive behavior associated with effective charge transport mechanisms within the composite materials. These measurements were performed across all tested formulations to determine the electrical percolation behavior. Once the percolation threshold is reached, σ' becomes almost frequency-independent, indicating that it closely approaches the true direct current (DC) conductivity. Figure 5 shows the electrical conductivity of the SEBS/CB and EVA/CB composites as a function of mass fraction, at a frequency of 1 Hz.

The percolation threshold for both SEBS/CB and EVA/CB composites was found to be ~12 wt%. Beyond this threshold, the electrical conductivity of both composites reached a plateau at about 0.01 S/m at 20 wt%. Below the percolation threshold, the measured conductivity is overestimated due to the influence of frequency-dependent mechanisms such as interfacial polarization and charge hopping, which do not reflect true DC conduction.

FIGURE 3 | Electrodes installed in the system for the acquisition of electrical signals from the brain. [Color figure can be viewed at wileyonlinelibrary.com]

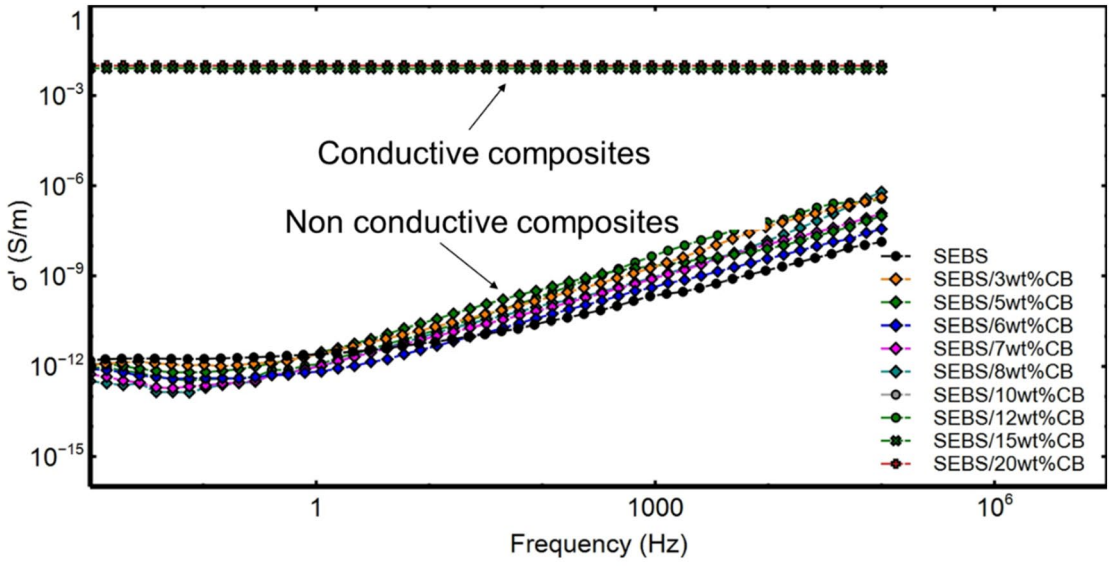

(a)

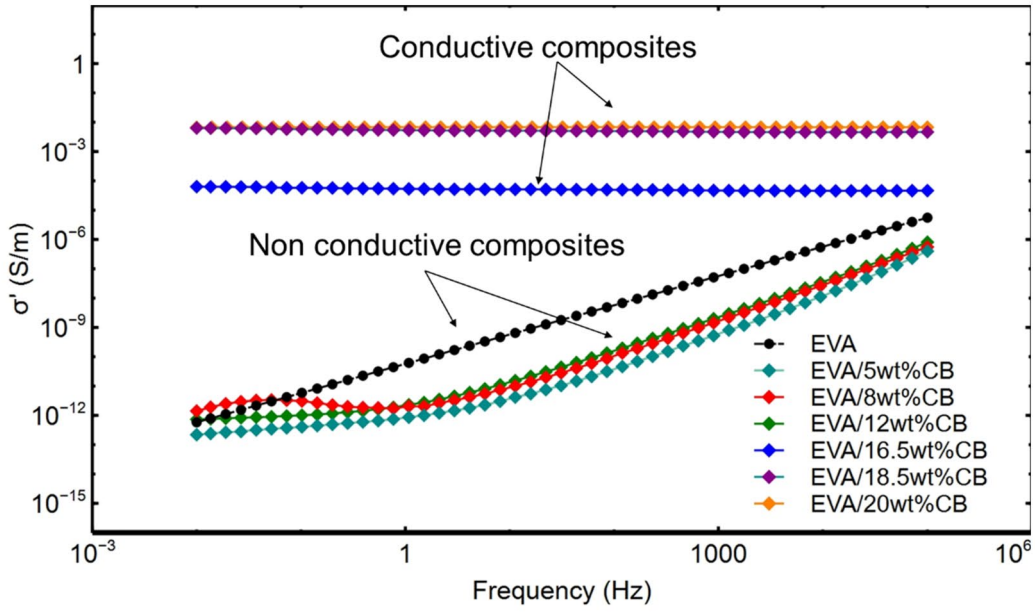

(b)

FIGURE 4 | Real part of the complex conductivity as a function of frequency of (a) SEBS/CB and (b) EVA/CB. [Color figure can be viewed at wileyonlinelibrary.com]

This behavior is visible in Figure 4a for concentrations below 15 wt% CB for SEBS/CB composite, and below 16.5 wt% CB, for EVA/CB composite in Figure 4b. It can also be seen in the non-conductive domain (0–12 wt%) that the value of the AC conductivity at a given frequency is not well correlated with the CB concentration. The composites with the highest mass fraction (SEBS/20 wt% CB and EVA/20 wt% CB) were chosen for the fabrication of the electrodes to perform the EEG measurements since, as could be expected, they have the highest electrical conductivities (0.01 S/m).

The evolution of the electrical conductivity of the composites as a function of the frequency in Figure 4 confirms that the percolation threshold of the SEBS/CB composites is below 15 wt% CB and that of the EVA/CB composites is below 16.5 wt% CB.

Figure 5 shows that the EVA/CB and SEBS/CB composites have the same percolation threshold (12 wt% CB).

The graph of Figure 5 depicts the electrical conductivity of SEBS/CB composites as a function of carbon black (CB) mass fraction, measured at 1 Hz. At low CB mass fractions (0–12 wt%), the conductivity remains extremely low, around 10^{-12} S/m, indicating insulating behavior. This suggests that CB particles are insufficiently connected to form conductive paths within the SEBS matrix. Around 12 wt% CB, there is a sharp increase in conductivity, spanning several orders of magnitude, reaching approximately 10^{-2} S/m. This marks the percolation threshold, where CB particles form a continuous network, enabling efficient electrical conduction. Beyond 15 wt% CB, the conductivity plateaus, showing no significant

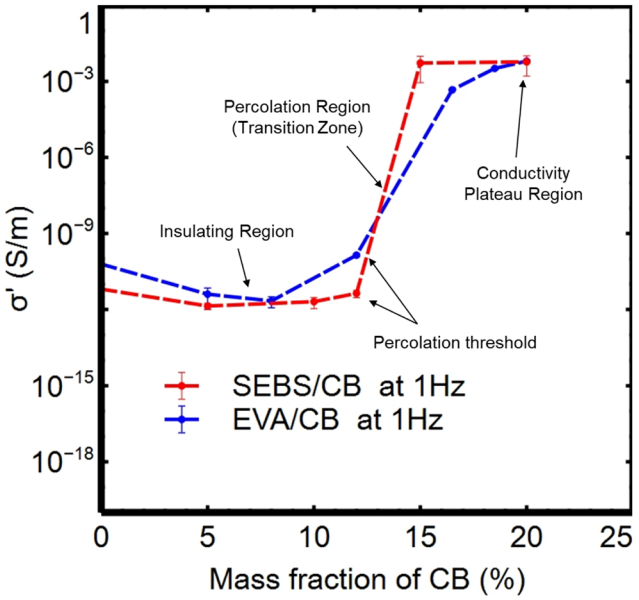

FIGURE 5 | Electrical conductivity as a function of mass fraction. [Color figure can be viewed at wileyonlinelibrary.com]

increase as the CB concentration increases further. This indicates that the conductive network has stabilized, and additional CB has a diminishing effect on further improving conductivity. The percolation threshold is observed near 12 wt% CB. The steepness of the conductivity increase at the percolation threshold demonstrates that CB particles form a well-distributed and interconnected network in the SEBS matrix, enhancing electrical properties efficiently. Below the percolation threshold, SEBS/CB composites are suitable for applications requiring insulating properties. Near or beyond the percolation threshold, the composites exhibit significant conductivity, making them suitable for EEG electrodes. The graph of Figure 4a demonstrates the percolation behavior of SEBS/CB composites, with a critical threshold near 12 wt% CB. Beyond this threshold, the material becomes conductive, suitable for flexible electronic applications. The results highlight the importance of achieving uniform filler dispersion and optimizing CB content for specific electrical properties.

The plot in Figure 4b shows the variation of electrical conductivity of EVA/CB (Ethylene-Vinyl Acetate/Carbon Black) composites as a function of the carbon black (CB) mass fraction, measured at 1 Hz. From 0% to 12%, the conductivity remains extremely low, around 10^{-12} S/m, indicating that the material is electrically insulating. In this range, the carbon black particles are too sparsely distributed to form conductive pathways. The composite behaves like a dielectric material. From 12% CB content, a significant increase in conductivity is observed, reaching a plateau of 10^{-2} S/m. This sharp rise is attributed to the percolation threshold, where CB particles form a continuous conductive network within the EVA matrix. From 16.5% to 20%, beyond the percolation threshold, the conductivity stabilizes at 10^{-2} S/m. Further increases in CB concentration enhance the density of the conductive network but do not drastically improve the conductivity as saturation is approached. Below 12% CB, composites have an insulating behavior due to isolated CB particles whereas above 12% CB, they have a conductive behavior due to interconnected CB particles. For flexible electrodes, a CB content above the percolation threshold (12%–20%) is necessary to ensure sufficient electrical conductivity for signal acquisition. Adjusting the CB content allows to tune the conductivity and mechanical properties in order to balance performance and flexibility. These findings confirm the need to carefully optimize the CB mass fraction to achieve the desired electrical properties in EVA/CB composites. A CB mass fraction of 12%–20% is ideal for applications requiring conductivity, such as dry EEG electrodes.

3.1.2 | Structural Properties

Figure 6 presents the scanning electron microscope (SEM) micrograph of SEBS/CB and EVA/CB composites containing 20 wt% CB. The results show that the CB particles appear to be well distributed at this concentration in both composites. The Figure 6 shows that due to the high concentration of carbon black (20 wt%) in the nanocomposites, some agglomerated particles were observed in SEBS/20 wt% CB and EVA/20 wt% CB. The agglomerations are indicated in Figure 6 as large CB in the SEBS/20 wt% CB and EVA/20 wt% CB samples. The interaction of the reinforcement (CB) inside the different matrices is also apparent. The presence of agglomerates is primarily attributed to the high CB concentration. Despite this, these agglomerates contribute to the formation of conductive paths within the composites through CB-CB contacts. As the CB concentration increases, these agglomerates become more interconnected, enhancing the density of the conductive network.

3.1.3 | Thermal Properties

To support the development of flexible dry EEG electrodes, DSC analysis was performed to assess whether adding carbon black influences the thermal stability and segmental mobility of the SEBS and EVA matrices. As shown in Figures 7 and 8, both composites retain the characteristic thermal signatures of their respective elastomers.

The SEBS/CB composite exhibits a glass-transition temperature (T_g) near −50°C, typical of the ethylene–butylene soft phase, with no melting or crystallization peaks across the heating and cooling cycles. This confirms the fully amorphous nature of SEBS and indicates that CB loading does not disturb its microphase-separated structure. The EVA/CB composite shows a T_g around −35°C, along with a broad endothermic transition above 80°C–90°C corresponding to the softening of the vinyl-acetate–rich domains.

These results demonstrate that the thermal transitions of both matrices remain essentially unchanged after CB incorporation. This is an important outcome for EEG electrode fabrication: the CB network enhances conductivity without compromising the thermal integrity or processing window of the elastomer. The composites, therefore, maintain the flexibility and thermal stability required for reliable, skin-conforming EEG electrodes while supporting improved electrical performance.

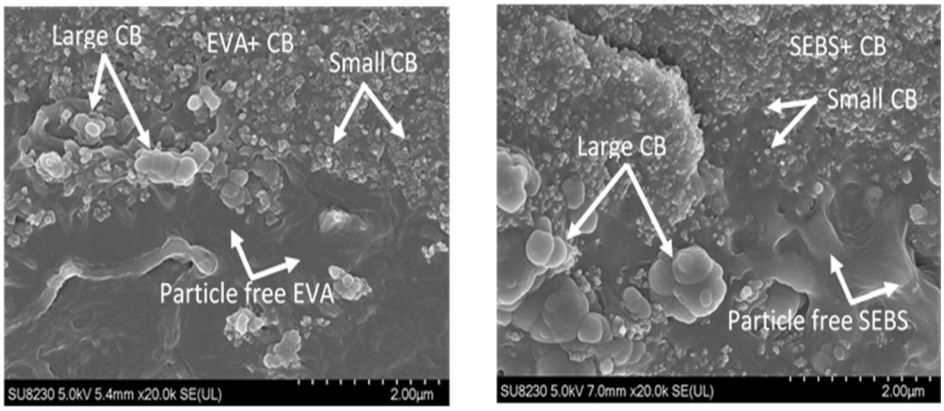

FIGURE 6 | Micrograph of both electrodes: (a) EVA/20 wt% CB and (b) SEBS/20 wt% CB.

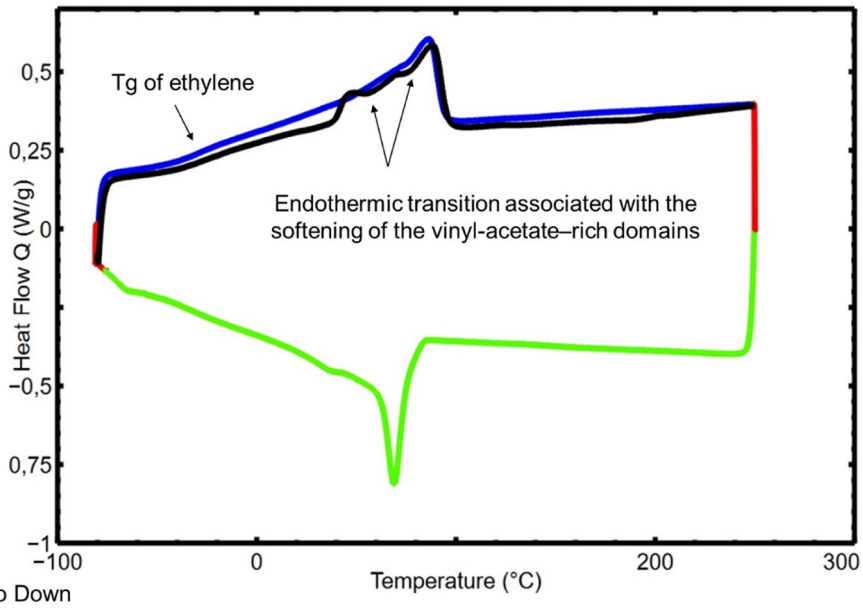

FIGURE 7 | Differential scanning calorimetry (DSC) thermogram of EVA/20 wt% CB composite. The second heating (blue) and cooling (green) curves display a glass transition around −30°C, a crystallization peak near 55°C–60°C, and a melting endotherm at approximately 95°C–100°C. [Color figure can be viewed at wileyonlinelibrary.com]

3.1.4 | Mechanical Properties

Figure 9 shows the results of cyclic compression tests performed on SEBS/20 wt % CB (green curve) and EVA/20 wt% CB (red curve).

The steeper slope of the stress–strain curve at the initial linear region indicates stiffness. EVA/20 wt% CB (red curve) shows a higher stiffness as compared to SEBS/20 wt% CB, suggesting that EVA/20 wt% CB is less deformable under compression. The loops in the curves indicate energy dissipation during loading and unloading (hysteresis). EVA/20 wt% CB exhibits larger hysteresis loops as compared to SEBS/20 wt% CB, indicating a greater energy loss, likely due to greater internal friction or viscoelastic effects. SEBS/20 wt% CB shows a narrower hysteresis loop, suggesting a better elastic recovery after compression as compared to EVA/20 wt% CB, which retains more deformation after unloading. EVA/20 wt% CB withstands a higher maximum stress at a given strain, showing greater resistance to deformation under load. However, SEBS/20 wt% CB achieves a higher strain at lower stress, demonstrating greater flexibility. SEBS/20 wt% CB is more flexible and better suited for applications requiring high deformation and recovery, such as wearable sensors or flexible electrodes. EVA/20 wt% CB, being stiffer, might be preferred for applications demanding higher structural integrity under load. To manufacture dry flexible EEG electrodes, SEBS/20 wt% CB is a better choice than EVA/20 wt% CB, based on the following key measured parameters, including: the stress at 50% extension, the elastic modulus, the hysteresis loss, the loading energy, and the energetic ratios across multiple cycles:

- The stress at 50% of EVA/20 wt% CB is 16.2 MPa, and that of SEBS/20 wt% CB is 9.35 MPa. EVA/20 wt% CB exhibits a higher stress at a 50% extension, indicating a greater resistance to deformation as compared to SEBS. This suggests

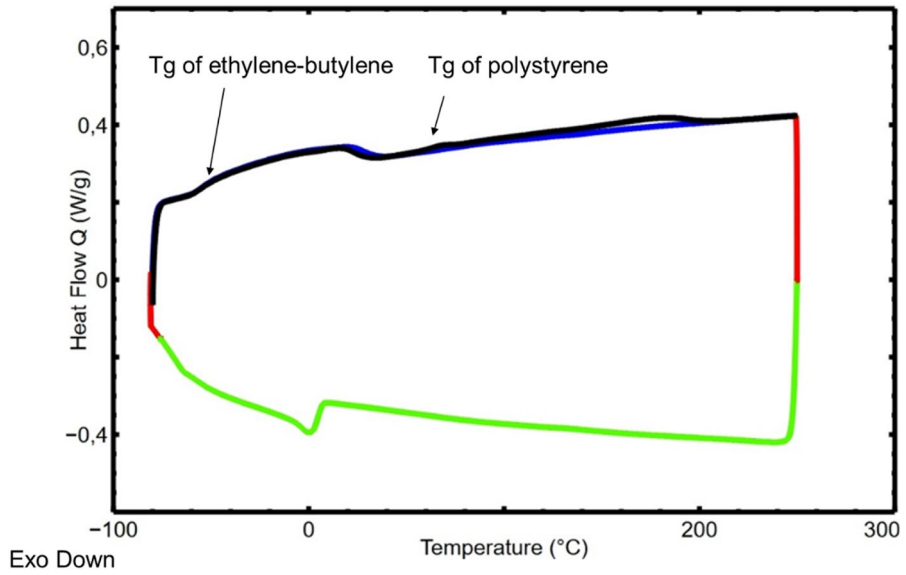

FIGURE 8 | Differential scanning calorimetry (DSC) thermogram of the SEBS/20 wt% CB composite. The curve shows a glass transition of the ethylene–butylene (EB) phase near −50°C, a weak transition of the polystyrene domains at 90°C–100°C. [Color figure can be viewed at wileyonlinelibrary.com]

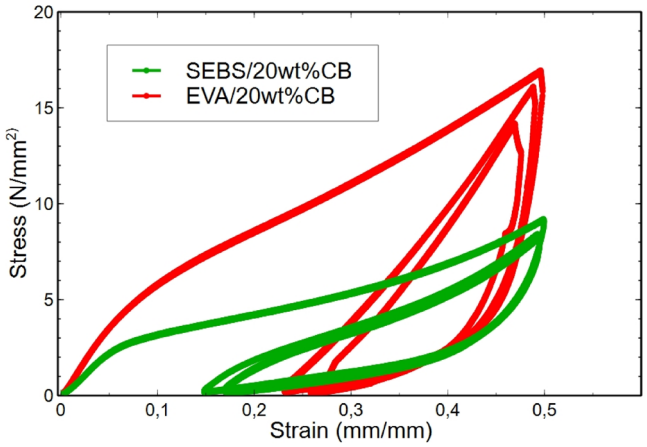

FIGURE 9 | Stress–strain behavior of SEBS/20 wt% CB and EVA/20 wt% CB under compression tests. [Color figure can be viewed at wileyonlinelibrary.com]

that EVA is more rigid, while SEBS/20 wt% CB is more flexible, making SEBS potentially more suitable for applications where flexibility and adaptability (conforming to curved surfaces) are essential.

- The elastic Modulus EVA/20 wt% CB is 63.8 MPa and that of SEBS/20 wt% CB is 47.2 MPa. EVA/20 wt% CB has a higher elastic modulus, confirming its greater rigidity. SEBS, with a lower elastic modulus, is softer and more elastic, which may provide better comfort and adaptability in flexible electrode applications such as EEG systems.
- The hysteresis Loss (Energy Dissipated as Heat) of EVA/20 wt% CB is Cycle 1: 27.2 J → Cycle 3: 7.63 J, and that of SEBS/20 wt% CB is Cycle 1: 13.3 J → Cycle 3: 5.17 J. EVA/20 wt% CB dissipates significantly more energy as heat than SEBS in all cycles. This decrease in energy values corresponds to the reduction of the area enclosed by the stress–strain hysteresis loops between the first and third loading–unloading cycles, indicating that the material dissipates less mechanical energy as heat as its internal structure becomes stabilized after repeated deformation. Both materials stabilize after repeated cycles, with the hysteresis loss decreasing by approximately 72% (EVA/20 wt% CB) and 61% (SEBS/20 wt% CB) from Cycle 1 to Cycle 3. SEBS demonstrates a lower energy dissipation overall, indicating greater efficiency and mechanical resilience.
- The loading Energy (Total Energy Absorbed) of EVA/20 wt% CB is Cycle 1: 32.79 J → Cycle 3: 12.78 J, and that of SEBS/20 wt% CB Cycle 1: 18.93 J → Cycle 3: 10.19 J. EVA/20 wt% CB absorbs more energy than SEBS/20 wt% CB, consistent with its higher rigidity and resistance to deformation. Both materials show reduced loading energy over cycles, reflecting material stabilization under repeated loading.
- The energetic Ratio (Energy Returned/Stored) of EVA/20 wt% CB is Cycle 1 = 82%, Cycle 2 = 63%, Cycle 3 = 59% and that of SEBS/20 wt% CB is Cycle 1 = 70%, Cycle 2 = 53%, Cycle 3 = 50%. EVA/20 wt% CB has higher energetic ratios in all cycles, meaning that it returns a higher proportion of absorbed energy. However, the ratio drops more significantly for EVA/20 wt% CB (23% reduction) than for SEBS/20 wt% CB (20% reduction) from Cycle 1 to Cycle 3. SEBS shows a more stable energy return behavior, although it is overall less efficient than EVA in energy restitution.

3.2 | Experimental Validation in Vivo

The contact impedance of the EVA/20 wt% CB electrode is 26.8 ± 4.4 kΩ. This high impedance, with significant variability (large standard deviation), indicates poor electrical contact with

the skin, which leads to reduced signal quality and increased noise during EEG measurements. The large variability suggests inconsistent performance, likely caused by inadequate interaction between the electrode and the skin. The same impedance of flexible commercial electrodes is 4.2 ± 0.5 kΩ. This is the lowest impedance, suggesting a highly consistent performance as compared to that of the EVA/20 wt% CB electrode. The minimal impedance ensures optimal signal quality, making it a benchmark for EEG applications. The contact impedance of the SEBS/20 wt% CB electrode is 5.4 ± 0.9 kΩ. This value is much lower than that of the EVA/20 wt% CB and close to that of the commercial electrode. The small standard deviation indicates consistent performance. The low impedance reflects a better electrode-skin interface and improved electrical conductivity, likely due to SEBS's flexibility and better dispersion of conductive fillers. Its low contact impedance makes it suitable for reliable EEG signal acquisition. Figure 10. shows the eye movement-related artifacts of SEBS/20 wt% CB, EVA/20 wt% CB, and commercial electrodes.

The eye movement-related artifacts plots in Figure 10, which show a comparison of the commercial dry flexible electrode, EVA/20 wt% CB, and SEBS/20 wt% CB, reveal notable differences in signal quality and stability.

- Commercial Dry Flexible Electrode (Top Panel—Blue Line): The signal is stable and clear, with amplitudes of ~±2000 μV. The consistent patterns during eyes-open and eyes-closed periods indicate good sensitivity to changes in brain activity. The commercial electrode provides reliable signal quality, serving as a benchmark for comparison.
- EVA/20 wt% CB Electrode (Middle Panel—Red Line): The signal shows amplitude spikes exceeding ±10,000 μV, particularly during transitions between eyes-open and eyes-closed states. These spikes suggest poor contact impedance and suboptimal electrode-skin contact, compromising signal reliability. When comparing the signal amplitudes recorded during the eyes-open phases, significantly larger amplitude fluctuations are observed with the EVA/20 wt% CB electrode compared to SEBS/20 wt% CB and PDMS (EVA/CB > SEBS/CB > Commercial Dry Flexible Electrode PDMS, with no fluctuations detected for the commercial electrode). These pronounced variations may account for the higher overall amplitude observed with EVA/CB.
- SEBS/20 wt% CB Electrode (Bottom Panel—Green Line): The signal amplitude is well-controlled and remains within ~±10,000 μV, reflecting a better contact impedance. The clear differentiation between eyes-open and eyes-closed states suggests that SEBS/20 wt% CB electrodes are capable of effectively capturing EEG signals.

To better contextualize the contribution of this work, Table 2 summarizes the performance of the newly developed SEBS/CB and EVA/CB electrodes in comparison with recently reported flexible dry and wet EEG electrodes. The comparison includes parameters such as material composition, fabrication method, contact impedance, electrical conductivity, mechanical compliance, and electrode type.

Table 2 clearly shows that while most PDMS- and TPU-based dry electrodes exhibit contact impedance values ranging from tens to several hundred kilo-ohms, the SEBS/CB composite developed in this study achieves a remarkably low impedance of approximately 5 kΩ, approaching that of commercial flexible electrodes. Furthermore, SEBS/CB combines this electrical performance with superior softness and elasticity, resulting in stable EEG signal acquisition and enhanced user comfort. The recyclability and processability of thermoplastic matrices such as SEBS and EVA also provide an additional advantage over conventional thermoset-based systems, enabling scalable, cost-effective manufacturing for wearable biosensors.

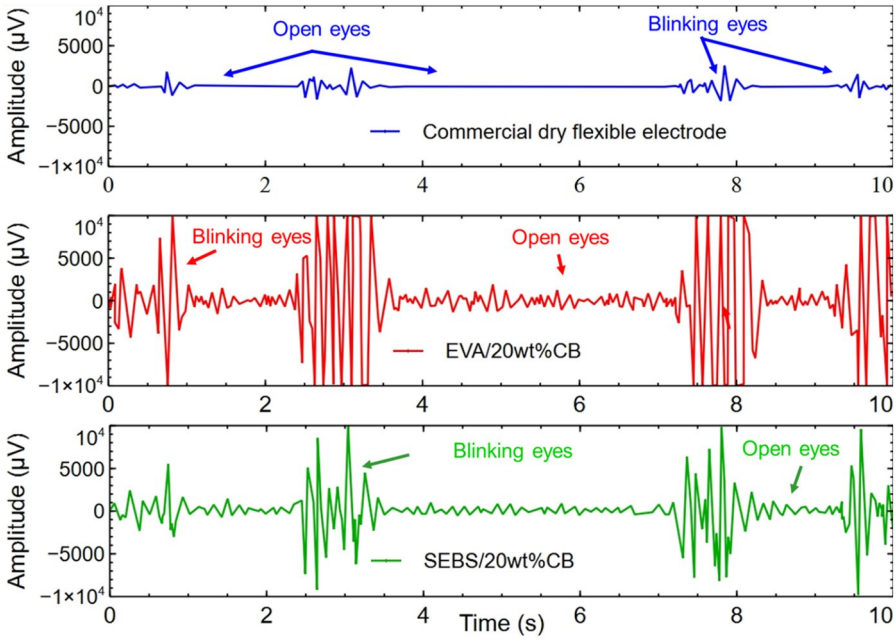

FIGURE 10 | EEG signals of SEBS/20 wt% CB, EVA/20 wt% CB, and commercial electrodes. [Color figure can be viewed at wileyonlinelibrary.com]

TABLE 2 | Comparison with relevant work in the application area.

Electrode material	Fabrication method	Contact impedance	References
PDMS/AgNWs	3D printing	10 kΩ at 1 kHz	[38]
PDMS/CNT	Sonication	290 kΩ at 10 Hz	[39]
PDMS/CNT	Sonication + magnetic stirring	9 kΩ	[40]
PDMS/CB	Sonication + magnetic stirring	18 kΩ at 10 Hz	[41]
PDMS/Au	Coating	18 kΩ at 20 Hz	[16]
PDMS/Cu	Coating	600 kΩ at 31 Hz	[42]
PDMS/Cu	Coating	39.43 kΩ	[43]
PDMS/CNT	Tree-roll milling	19–38 kΩ at 1 kHz	[30]
PDMS/MWCNTs	Sonication	250 kΩ at 30 Hz	[31]
PDMS/Ag/CNT-GO	Coating	6.4–7.2 kΩ	[44]
PU/Ni/Cu	Coating	2000 kΩ	[45]
PU/Ag/AgCl	Coating	702 ± 219 kΩ	[46]
PU/CB	3D printing	70–90 kΩ at 30 Hz	[47]
PU/Ag/AgCl	Coating	264 ± 125 kΩ	[48]
PU/Ag/AgCl	Coating	601.5 ± 400.8 kΩ	[27]
EVA/CB	Magnetic stirring	26.8 ± 4.4 kΩ at 31 Hz	This work
SEBS/CB	Magnetic stirring	5.4 ± 0.9 kΩ at 31 Hz	This work
Commercial flexible electrodes	—	4.2 ± 0.5 kΩ at 31 Hz	This work

4 | Discussion

This study aimed to evaluate the electrical and mechanical performance of flexible dry electrodes based on SEBS/CB and EVA/CB for EEG signal acquisition, comparing them with commercial flexible dry electrodes. The results highlight several key findings regarding electrical conductivity, mechanical properties, contact impedance, and EEG signal quality. The percolation threshold for both SEBS/CB and EVA/CB composites was found to be identical, with both materials exhibiting comparable bulk electrical conductivity once a continuous carbon-black network is established. Below this threshold, incomplete pathways lead to high resistivity, while approaching it produces the expected sharp rise in conductivity associated with classical percolation behavior. Above the threshold, conductivity continues to improve as additional CB densifies the existing network; however, excessive loading increases mixture viscosity, promotes agglomeration, and restricts polymer chain mobility. These effects can limit conductivity gains and decrease elasticity by introducing stiffness. For flexible dry EEG electrodes, such stiffening is undesirable, as it reduces skin conformity and comfort. This highlights the need for an optimal CB concentration that provides a robust conductive network without compromising the mechanical compliance required for wearable bioelectronic applications.

However, the electrical conductivity plateau achieved by the composites developed in this study is approximately one order of magnitude lower than that reported in similar studies using melt-mixed SEBS/CB composites, such as the work by Kuester et al. [49]. Similar effects of CB dispersion and network morphology on conductivity development have been reported by Jamatia et al. [50] reported an electrical conductivity of 0.01 S/m for SEBS/CB composites prepared via the toluene dissolution method with a very high filler content of 70 vol%. Conversely, SEBS-based composites containing 5 wt% of carbon black (CB) fabricated through extrusion, as reported by Lakto et al. [51], exhibited a significantly lower conductivity of 0.0001 S/m. These comparisons suggest that the processing method, filler dispersion, and polymer-filler interactions critically influence the final electrical performance of the composites. As reported in previous studies [52–55] and as confirmed by the findings of this work, the variation in electrical conductivity as a function of conductive filler concentration can be generally divided into three distinct regions. In the insulating region, corresponding to low filler content, the AC conductivity strongly depends on frequency. As the CB content increases and approaches the percolation threshold, a sharp rise in conductivity is observed. Beyond this threshold, the AC conductivity becomes almost frequency-independent, indicating the formation of a continuous conductive network within the polymer matrix. At this stage, the composite behaves as an electrically conductive material [56]. In addition, recent works on conductive polymer composites and EMI-shielding materials provide valuable insight into the structure–property relationship of similar systems. For example, hybrid and hierarchical composites based on MXene, CNTs, or π-conjugated polymers have been shown to enhance both conductivity and

flexibility through synergistic filler dispersion and strong interfacial bonding [57–61]. Furthermore, MAX-phase-based and core–shell magnetic filler systems enhance electromagnetic absorption and mechanical resilience, highlighting the significance of filler architecture in energy dissipation and mechanical reinforcement [62–64].

SEM micrographs revealed a homogeneous dispersion of CB particles, but agglomerations were present at higher CB loadings (20 wt%), particularly in both SEBS/CB and EVA/CB composites. Similar agglomerations were reported in [51, 52] due to the high concentration of carbon black. While these agglomerations can lead to some variations in conductivity, they also contribute to the formation of percolating networks necessary for efficient charge transport. The presence of CB-CB contacts ensures that conductive paths are present inside the polymer matrix, supporting the electrical performance.

EVA/20 wt% CB is stiffer and more resistant to deformation, with higher stress and modulus, whereas SEBS/20 wt% CB is softer and more elastic, offering better adaptability and comfort. SEBS/20 wt% CB dissipates less energy as heat, resulting in lower hysteresis loss, and is more mechanically resilient under repeated loading cycles. Both materials stabilize over cycles, but SEBS/20 wt% CB demonstrates better overall consistency in energy absorption and dissipation. EVA/20 wt% CB is suitable for applications requiring rigidity and higher energy restitution. However, its higher hysteresis losses and reduced stability may limit performance under repeated mechanical loads. SEBS/20 wt% CB is better suited for applications where flexibility, comfort, and mechanical durability are essential, such as flexible EEG electrodes. Its lower hysteresis loss and higher resilience under repeated use make it a more reliable choice. SEBS/20 wt% CB has a lower stiffness, indicated by the gentler slope of the stress–strain curve, making it more flexible and better able to conform to scalp contours, thus enhancing user comfort. The narrower hysteresis loop for SEBS/20 wt% CB signifies better elastic recovery, ensuring the electrode maintains good skin contact after repeated compression, which is vital for long-term EEG monitoring. Known for its biocompatibility, SEBS is safer for direct skin contact, reducing the risk of irritation or discomfort. The lower stress at the same strain decreases the risk of discomfort or pressure-related issues during prolonged use. Conversely, EVA/20 wt% CB's higher stiffness may limit its ability to conform to scalp curves, potentially leading to poor contact and increased impedance at the skin-electrode interface. Its larger hysteresis suggests less adaptability and greater discomfort over extended periods. Overall, SEBS/20 wt% CB is the preferred material for dry, flexible EEG electrodes, as its superior flexibility ensures better skin-electrode contact, lower impedance, and more reliable signal acquisition. Similar behavior has been observed in other thermoplastic elastomer nanocomposites and EOC-based foams, which exhibited improved cyclic compression recovery and reduced hysteresis when reinforced with comparable filler content [65]. The current results also align with those of Wang et al. [60], and Ugraskan et al. [64], where carbon-based or SWCNT-reinforced polymer composites demonstrated improved conductivity and compressive recovery due to efficient filler–matrix adhesion. Similarly, PVDF- and polyurethane-based nanocomposites exhibit balanced conductivity and flexibility [63, 66], while hybrid systems integrating graphene, nanodiamond, or MXene phases show outstanding EMI shielding and mechanical durability [67, 68]. Overall, these results confirm that the interplay between filler dispersion, interfacial adhesion, and matrix elasticity governs the electrical and mechanical response of SEBS/CB and EVA/CB composites. SEBS/20 wt% CB, in particular, provides an optimal balance of conductivity, softness, and resilience, making it an excellent candidate for durable and comfortable dry EEG electrodes. The superior flexibility of the SEBS/CB electrodes makes them particularly suitable for EEG applications, ensuring better conformity to the scalp curvature and reducing motion artifacts.

The DSC thermograms of the SEBS/CB and EVA/CB composites provide additional insight into the thermal stability and segmental mobility of the elastomer matrices after the incorporation of carbon black. Both materials retain their characteristic thermal transitions, indicating that the filler does not alter the intrinsic thermal behavior of the polymers. SEBS/CB exhibits a glass transition near −50°C, consistent with the soft ethylene–butylene phase, while EVA/CB shows a T_g around −35°C followed by a mild endothermic transition associated with the softening of the vinyl-acetate-rich domains. These observations confirm that the addition of 20 wt% carbon black does not disrupt the microphase structure or thermal relaxation mechanisms of either matrix. This is particularly relevant for EEG applications, as the preservation of the thermal transitions ensures that the composites maintain the elasticity, softness, and temperature resilience required for skin-conforming electrodes. The stable thermal behavior supports the conclusion that the improvements in electrical conductivity and mechanical response reported in this study arise primarily from the formation and densification of the CB conductive network, rather than from modifications of the polymer thermal properties.

The comparative results highlight that the SEBS/CB electrode developed in this work offers the best trade-off between conductivity, impedance, flexibility, and manufacturability among polymer-based dry electrodes reported to date. Its performance is close to that of commercial reference electrodes, demonstrating the effectiveness of carbon black dispersion and the suitability of SEBS as a soft, recyclable matrix for EEG applications. EVA/CB electrodes, while less flexible, still outperform many PDMS- and TPU-based counterparts in terms of impedance and cost-effectiveness. These findings confirm the potential of SEBS- and EVA-based composites as sustainable alternatives for large-scale fabrication of comfortable and durable EEG electrodes.

The stability of flexible dry electrodes over time is vital for reliable EEG signal acquisition. In this study, measurements were taken over a 10-s recording period, which aligns with durations reported in previous research using the same timeframe [69–72]. During this period, both SEBS/CB and EVA/CB electrodes showed consistent impedance and signal amplitude, confirming their short-term stability. Although the in vivo evaluation provided useful insights into the real-world performance of the electrodes, certain limitations must be recognized. The study involved four participants, and the EEG recordings lasted only 10 s, which limits the statistical

significance of the findings. Future research will involve larger participant groups, longer recording sessions, and additional analyses in both time and frequency domains to verify the robustness of the observed performance. These efforts will also assist in validating the long-term stability and clinical potential of SEBS-based electrodes for wearable and medical-grade EEG monitoring.

SEBS/CB electrodes exhibited significantly lower contact impedance than EVA/CB electrodes, as well as those made of TPU and PDMS discussed in this paper. The EEG signal analysis further supports the superiority of SEBS/CB electrodes over EVA/CB. SEBS/20 wt% CB electrodes are preferred for flexible EEG applications due to their lower contact impedance and more stable signal performance as compared to EVA/20 wt% CB. The signal waveforms highlight the significant role of contact impedance in ensuring stable and high-quality signal acquisition. Contact impedance, a key parameter influencing EEG signal quality, is critical for evaluating electrode performance. Compared to the SEBS/CB and EVA/CB electrodes developed in this study, the active claw-shaped dry electrodes proposed by Wang et al. [28] exhibit significantly higher and less stable contact impedance, particularly over hairy scalp areas. Similarly, other flexible, low-cost dry electrodes reported in the literature [73–75] also present higher contact impedance relative to the SEBS/CB electrodes developed in this work, further demonstrating the superior electrical performance of the latter. This superior performance is attributed to the improved skin-electrode interface stability and the lower impedance achieved with the SEBS/CB formulation, which is particularly beneficial for reliable and high-quality EEG signal acquisition. Furthermore, both SEBS/CB and EVA/CB electrodes outperform the silicone-based dry electrodes fabricated by Han et al. [43] and Stauffer et al. [18] in terms of contact impedance, underscoring their enhanced electrical properties and more stable skin-electrode coupling. These findings underscore that contact impedance, alongside bulk electrical conductivity, is a critical parameter in the design and fabrication of effective EEG electrodes. The results clearly demonstrate that contact impedance, rather than electrical conductivity alone, plays a dominant role in determining EEG signal quality. This study highlights the strong potential of SEBS/CB electrodes as a superior alternative to conventional materials such as EVA for flexible EEG applications. SEBS/CB electrodes exhibit low contact impedance, excellent flexibility, and deliver a stable EEG signal acquisition. Nevertheless, there remains room for further improvements, particularly in optimizing the electrode-skin interface, enhancing long-term stability, and refining manufacturing processes to scale production while maintaining performance. Further improvements can be explored:

- Optimizing SEBS/CNT composites: Carbon nanotube (CNT) reinforcements could enhance conductivity without significantly increasing stiffness.
- Evaluating long-term stability: Investigating the durability of SEBS/CB electrodes under prolonged use and repeated compression cycles.
- Improving skin adhesion: Future designs could incorporate self-adhesive materials or integrate the electrodes into EEG headsets for better stability and reduced motion artifacts.
- Exploring hybrid composites: Combining SEBS with additional conductive fillers (e.g., CB, graphene, CNT) could further reduce the impedance and enhance the signal quality.

5 | Conclusions

This study provided a comprehensive comparison between flexible dry EEG electrodes fabricated from SEBS/CB and EVA/CB conductive polymer composites, emphasizing their electrical, mechanical, and functional performance. Both composites achieved a bulk electrical conductivity of approximately 0.01 S/m with a percolation threshold near 12 wt% carbon black. However, SEBS/CB electrodes exhibited significantly lower contact impedance ($5.4 \pm 0.9\,k\Omega$) compared to EVA/CB ($26.7 \pm 4.4\,k\Omega$), approaching the performance of a commercial flexible electrode ($4.2 \pm 0.5\,k\Omega$).

From a mechanical perspective, SEBS/CB demonstrated greater softness, elasticity, and energy efficiency, leading to improved scalp conformity and reduced hysteresis loss during cyclic deformation. In contrast, EVA/CB exhibited higher rigidity and energy dissipation, consistent with its thermoplastic character. EEG recordings further confirmed that SEBS/CB electrodes produced more stable and higher-quality signals, whereas EVA/CB performance was limited by higher impedance and lower flexibility.

Overall, the results indicate that SEBS/CB composites provide the most balanced combination of electrical performance, mechanical compliance, and user comfort, making them promising materials for durable, high-performance, and comfortable dry EEG electrodes.

Nevertheless, some limitations should be acknowledged: the number of in vivo tests was limited, the measurements were restricted to short-term recordings, and long-term stability or large-scale reproducibility was not yet evaluated. These aspects will be addressed in future work through extended testing across multiple participants and under dynamic, real-world conditions to confirm the robustness and reliability of the developed electrodes.

Future studies will include extended EEG sessions and SNR- and frequency-domain analyses to quantitatively evaluate signal fidelity, amplitude stability, and overall performance of SEBS- and EVA-based electrodes under different operating conditions.

Author Contributions

George Gnonhoue: formal analysis (lead), investigation (lead), methodology (lead), software (lead), validation (lead), visualization (lead), writing – original draft (lead), writing – review and editing (lead). **Ilyass Tabiai:** conceptualization (lead), funding acquisition (lead), resources (lead), supervision (lead). **Jérémie Voix:** conceptualization (lead), funding acquisition (lead), project administration (lead), supervision (lead), writing – review and editing (lead). **Éric David:** conceptualization (lead), funding acquisition (lead), supervision (lead), writing – review and editing (lead).

Acknowledgments

The authors would like to acknowledge the financial support received from NSERC Alliance (ALLRP 566678-2021), MITACS IT26677 (SUBV-2021-168), and PROMPT (#164_Voix-EERS 2021.06) for the ÉTS-EERS

Industrial Research Chair in In-Ear Technologies, which is sponsored by EERS Global Technologies Inc.

Funding

This work was supported by NSERC Alliance, ALLRP 566678-2021, Mitacs, MITACS IT26677 (SUBV-2021-168), and PROMPT, PROMPT (#164_Voix-EERS 2021.06).

Conflicts of Interest

The authors declare no conflicts of interest.

Data Availability Statement

The data that support the findings of this study are available on request from the corresponding author. The data are not publicly available due to privacy or ethical restrictions.

References

1. M. Arai, Y. Nishinaka, and N. Miki, "Electroencephalogram Measurement Using Polymer-Based Dry Microneedle Electrode," *Japanese Journal of Applied Physics* 54 (2015): 06FP14, https://doi.org/10.7567/JJAP.54.06FP14.

2. L. T. Cunha, P. Pedrosa, C. J. Tavares, E. Alves, F. Vaz, and C. Fonseca, "The Role of Composition, Morphology and Crystalline Structure in the Electrochemical Behaviour of TiNx Thin Films for Dry Electrode Sensor Materials," *Electrochimica Acta* 55 (2009): 59–67, https://doi.org/10.1016/j.electacta.2009.08.004.

3. Y. Fu, J. Zhao, Y. Dong, and X. Wang, "Dry Electrodes for Human Bioelectrical Signal Monitoring," *Sensors* 20 (2020): 3651, https://doi.org/10.3390/s20133651.

4. S. Krachunov and A. Casson, "3D Printed Dry EEG Electrodes," *Sensors* 16 (2016): 1635, https://doi.org/10.3390/s16101635.

5. P. S. Das, S. H. Park, K. Y. Baik, J. W. Lee, and J. Y. Park, "Thermally Reduced Graphene Oxide-Nylon Membrane Based Epidermal Sensor Using Vacuum Filtration for Wearable Electrophysiological Signals and Human Motion Monitoring," *Carbon* 158 (2020): 386–393, https://doi.org/10.1016/j.carbon.2019.11.001.

6. P. Fiedler, P. Pedrosa, S. Griebel, et al., "Novel Multipin Electrode Cap System for Dry Electroencephalography," *Brain Topography* 28 (2015): 647–656, https://doi.org/10.1007/s10548-015-0435-5.

7. S. Leach, K. Chung, L. Tüshaus, R. Huber, and W. Karlen, "A Protocol for Comparing Dry and Wet EEG Electrodes During Sleep," *Frontiers in Neuroscience* 14 (2020): 586.

8. N. V. de Camp, G. Kalinka, and J. Bergeler, "Light-Cured Polymer Electrodes for Non-Invasive EEG Recordings," *Scientific Reports* 8 (2018): 14041, https://doi.org/10.1038/s41598-018-32304-6.

9. H.-L. Peng, J.-Q. Liu, Y.-Z. Dong, B. Yang, X. Chen, and C.-S. Yang, "Parylene-Based Flexible Dry Electrode for Bioptential Recording," *Sensors and Actuators B: Chemical* 231 (2016): 1–11, https://doi.org/10.1016/j.snb.2016.02.061.

10. Y. Li, W. Zhou, C. Liu, et al., "Fabrication and Characteristic of Flexible Dry Bioelectrodes With Microstructures Inspired by Golden Margined Century Plant Leaf," *Sensors and Actuators A: Physical* 321 (2021): 112397, https://doi.org/10.1016/j.sna.2020.112397.

11. A. K. Srivastava, B. Bhartia, K. Mukhopadhyay, and A. Sharma, "Long Term Biopotential Recording by Body Conformable Photolithography Fabricated Low Cost Polymeric Microneedle Arrays," *Sensors and Actuators A: Physical* 236 (2015): 164–172, https://doi.org/10.1016/j.sna.2015.10.041.

12. H. J. Baek, H. J. Lee, Y. G. Lim, and K. S. Park, "Conductive Polymer Foam Surface Improves the Performance of a Capacitive EEG Electrode," *IEEE Transactions on Biomedical Engineering* 59 (2012): 3422–3431, https://doi.org/10.1109/TBME.2012.2215032.

13. A. A. Chlaihawi, B. B. Narakathu, S. Emamian, B. J. Bazuin, and M. Z. Atashbar, "Development of Printed and Flexible Dry ECG Electrodes," *Sensing and Bio-Sensing Research* 20 (2018): 9–15, https://doi.org/10.1016/j.sbsr.2018.05.001.

14. P. Fiedler, R. Muhle, S. Griebel, et al., "Contact Pressure and Flexibility of Multipin Dry EEG Electrodes," *IEEE Transactions on Neural Systems and Rehabilitation Engineering* 26 (2018): 750–757, https://doi.org/10.1109/TNSRE.2018.2811752.

15. C. Wehrmann, M. Langer, and M. Schilling, "Motion Artefact Detection in Capacitively Coupled EEG Recording," *Biomedical Engineering* 58 (2013): 4165, https://doi.org/10.1515/bmt-2013-4165.

16. L.-F. Wang, J.-Q. Liu, B. Yang, and C.-S. Yang, "PDMS-Based Low Cost Flexible Dry Electrode for Long-Term EEG Measurement," *IEEE Sensors Journal* 12 (2012): 2898–2904, https://doi.org/10.1109/JSEN.2012.2204339.

17. S. M. A. Iqbal, I. Mahgoub, E. Du, M. A. Leavitt, and W. Asghar, "Advances in Healthcare Wearable Devices," *npj Flexible Electronics* 5 (2021): 9, https://doi.org/10.1038/s41528-021-00107-x.

18. F. Stauffer, M. Thielen, C. Sauter, et al., "Skin Conformal Polymer Electrodes for Clinical ECG and EEG Recordings," *Advanced Healthcare Materials* 7 (2018): 1700994, https://doi.org/10.1002/adhm.201700994.

19. G. Li, Z. Deng, M. Cai, et al., "A Stretchable and Adhesive Ionic Conductor Based on Polyacrylic Acid and Deep Eutectic Solvents," *npj Flexible Electronics* 5 (2021): 23, https://doi.org/10.1038/s41528-021-00118-8.

20. N. Cui, Y. Song, C.-H. Tan, et al., "Stretchable Transparent Electrodes for Conformable Wearable Organic Photovoltaic Devices," *npj Flexible Electronics* 5 (2021): 31, https://doi.org/10.1038/s41528-021-00127-7.

21. S. Raspopovic, G. Valle, and F. M. Petrini, "Sensory Feedback for Limb Prostheses in Amputees," *Nature Materials* 20 (2021): 925–939, https://doi.org/10.1038/s41563-021-00966-9.

22. M. Hassan, G. Abbas, N. Li, et al., "Significance of Flexible Substrates for Wearable and Implantable Devices: Recent Advances and Perspectives," *Advanced Materials Technologies* 7 (2022): 2100773, https://doi.org/10.1002/admt.202100773.

23. W. Heng, S. Solomon, and W. Gao, "Flexible Electronics and Devices as Human–Machine Interfaces for Medical Robotics," *Advanced Materials* 34 (2022): 2107902, https://doi.org/10.1002/adma.202107902.

24. S.-J. Park, M.-H. Kim, and T.-J. Ha, "All-Printed Wearable Humidity Sensor With Hydrophilic Polyvinylpyrrolidone Film for Mobile Respiration Monitoring," *Sensors and Actuators B: Chemical* 394 (2023): 134395, https://doi.org/10.1016/j.snb.2023.134395.

25. B.-C. Kang, B.-S. Park, and T.-J. Ha, "Highly Sensitive Wearable Glucose Sensor Systems Based on Functionalized Single-Wall Carbon Nanotubes With Glucose Oxidase-Nafion Composites," *Applied Surface Science* 470 (2019): 13–18, https://doi.org/10.1016/j.apsusc.2018.11.101.

26. Y. Li, M. Zhao, Y. Yan, et al., "Multifunctional Biomimetic Tactile System via a Stick-Slip Sensing Strategy for Human–Machine Interactions," *npj Flexible Electronics* 6 (2022): 46, https://doi.org/10.1038/s41528-022-00183-7.

27. J. J. A. Heijs, R. J. Havelaar, P. Fiedler, R. J. A. Van Wezel, and T. Heida, "Validation of Soft Multipin Dry EEG Electrodes," *Sensors* 21 (2021): 6827, https://doi.org/10.3390/s21206827.

28. Z. Wang, Y. Ding, W. Yuan, H. Chen, W. Chen, and C. Chen, "Active Claw-Shaped Dry Electrodes for EEG Measurement in Hair Areas," *Bioengineering* 11 (2024): 276, https://doi.org/10.3390/bioengineering11030276.

29. L. Xing and A. J. Casson, "3D-Printed, Directly Conductive and Flexible Electrodes for Personalized Electroencephalography," *Sensors and Actuators A: Physical* 349 (2023): 114062, https://doi.org/10.1016/j.sna.2022.114062.

30. J. Oh, K.-W. Nam, W.-J. Kim, B.-H. Kang, and S.-H. Park, "Flexible Dry Electrode Based on a Wrinkled Surface That Uses Carbon Nanotube/Polymer Composites for Recording Electroencephalograms," *Materials* 17 (2024): 668, https://doi.org/10.3390/ma17030668.

31. P. Sharma, S. Baloda, D. Verma, V. Janyani, R. Sharma, and N. Gupta, "Multiwall Carbon Nanotube/Polydimethylsiloxane Composites-Based Dry Electrodes for Bio-Signal Detection," *IEEE Journal on Flexible Electronics* 3 (2024): 108–114, https://doi.org/10.1109/JFLEX.2024.3367648.

32. P. Costa, S. Ribeiro, G. Botelho, A. V. Machado, and S. Lanceros Mendez, "Effect of Butadiene/Styrene Ratio, Block Structure and Carbon Nanotube Content on the Mechanical and Electrical Properties of Thermoplastic Elastomers After UV Ageing," *Polymer Testing* 42 (2015): 225–233, https://doi.org/10.1016/j.polymertesting.2015.02.002.

33. E. Tekay, B. Aybakan, and V. U. Aslan, "4D Printable Maleated Poly(Styrene-b-Ethylene/Butylene-b-Styrene) / Poly(Ethylene-Co-Vinyl Acetate) Thermoplastic Elastomer Blends; Effects of Blend Composition on Shape Memory and Mechanical Properties," *Additive Manufacturing* 78 (2023): 103870, https://doi.org/10.1016/j.addma.2023.103870.

34. Y.-J. Park, H.-S. Joo, H.-J. Kim, and Y.-K. Lee, "Adhesion and Rheological Properties of EVA-Based Hot-Melt Adhesives," *International Journal of Adhesion and Adhesives* 26 (2006): 571–576, https://doi.org/10.1016/j.ijadhadh.2005.09.004.

35. J. Guo, H. Wang, C. Zhang, Q. Zhang, and H. Yang, "MPPE/SEBS Composites With Low Dielectric Loss for High-Frequency Copper Clad Laminates Applications," *Polymers* 12 (2020): 1875, https://doi.org/10.3390/polym12091875.

36. M. Shafiee and A. Ramazani, "Investigation of Barrier Properties of Poly(Ethylene Vinyl Acetate)/Organoclay Nanocomposite Films Prepared by Phase Inversion Method," *Macromolecular Symposia* 274 (2008): 1–5, https://doi.org/10.1002/masy.200851401.

37. S. R. Sinha, L. Sullivan, D. Sabau, et al., "American Clinical Neurophysiology Society Guideline 1: Minimum Technical Requirements for Performing Clinical Electroencephalography," *Journal of Clinical Neurophysiology* 33 (2016): 303–307, https://doi.org/10.1097/WNP.0000000000000308.

38. Z. Wang, C. Chen, W. Li, et al., "A Multichannel EEG Acquisition System With Novel ag NWs/PDMS Flexible Dry Electrodes," *Annu Int Conf IEEE Eng Med Biol Soc* 2018 (2018): 1299–1302, https://doi.org/10.1109/EMBC.2018.8512563.

39. P. Burgar, Design of Flexible Dry CNT/PDMS Electrodes for In-Ear EEG.

40. J. Sanguantrakul, A. Hemakom, T. Soonrach, and P. Israsena, "PDMS/CNT Electrodes With Bioamplifier for Practical In-The-Ear and Conventional Biosignal Recordings," *Journal of Neural Engineering* 21 (2024): 056017, https://doi.org/10.1088/1741-2552/ad7905.

41. X. Cheng, C. Bao, X. Wang, F. Zhang, and W. Dong, "Soft Surface Electrode Based on PDMS-CB Conductive Polymer for Electrocardiogram Recordings," *Applied Physics A* 125 (2019): 876, https://doi.org/10.1007/s00339-019-3124-5.

42. Y. Meng, Z. Li, and J. Chen, "A Flexible Dry Electrode Based on APTES-Anchored PDMS Substrate for Portable ECG Acquisition System," *Microsystem Technologies* 22 (2016): 2027–2034, https://doi.org/10.1007/s00542-015-2490-y.

43. C.-H. Han, S.-U. Kim, K.-S. Lim, et al., "Evaluation of a Silicone-Based Flexible Dry Electrode for Measuring Human Bioelectrical Signals," *Biomedical Engineering Letters* 15 (2025): 563–574, https://doi.org/10.1007/s13534-025-00471-x.

44. P. Li, C. Wang, M. Li, X. Xuan, B. Zhou, and H. Li, "Flexible Silver/Carbon Nanotube-Graphene Oxide-Polydimethylsiloxane Electrode Patch for Electroencephalography Language," *Advanced Intelligent Systems* 5 (2023): 2300018, https://doi.org/10.1002/aisy.202300018.

45. H. J. Baek, H. S. Kim, J. Heo, Y. G. Lim, and K. S. Park, "Brain–Computer Interfaces Using Capacitive Measurement of Visual or Auditory Steady-State Responses," *Journal of Neural Engineering* 10 (2013): 024001, https://doi.org/10.1088/1741-2560/10/2/024001.

46. I. F. Warsito, M. Komosar, M. A. Bernhard, P. Fiedler, and J. Haueisen, "Flower Electrodes for Comfortable Dry Electroencephalography," *Scientific Reports* 13 (2023): 16589, https://doi.org/10.1038/s41598-023-42732-8.

47. L. Xing and A. J. Casson, "Directly Conductive, Flexible, 3D Printed, EEG Electrodes," in *Proceedings of the 2022 IEEE International Conference on Flexible and Printable Sensors and Systems (FLEPS)* (IEEE, 2022), 1–4.

48. B. Vasconcelos, P. Fiedler, R. Machts, J. Haueisen, and C. Fonseca, "The Arch Electrode: A Novel Dry Electrode Concept for Improved Wearing Comfort," *Frontiers in Neuroscience* 15 (2021): 748100, https://doi.org/10.3389/fnins.2021.748100.

49. S. Kuester, C. Merlini, G. M. O. Barra, et al., "Processing and Characterization of Conductive Composites Based on Poly(Styrene-b-Ethylene-Ran-Butylene-b-Styrene) (SEBS) and Carbon Additives: A Comparative Study of Expanded Graphite and Carbon Black," *Composites Part B, Engineering* 84 (2016): 236–247, https://doi.org/10.1016/j.compositesb.2015.09.001.

50. T. Jamatia, J. Matyas, R. Olejnik, et al., "Wearable and Stretchable SEBS/CB Polymer Conductive Strand as a Piezoresistive Strain Sensor," *Polymers* 15 (2023): 1618, https://doi.org/10.3390/polym15071618.

51. P. Latko, A. Bogucka, and A. Boczkowska, "Characterization of Thermoplastic Elastomers Based Composites Doped With Carbon Black," *International Journal of Mechanical Engineering and Automation* 2 (2015): 171–176.

52. S. Pavlovsky and A. Siegmann, "Chemical Sensing Materials. I. Electrically Conductive SEBS Copolymer Systems," *Journal of Applied Polymer Science* 113 (2009): 3322–3329, https://doi.org/10.1002/app.30310.

53. M. Arjmand, M. Mahmoodi, S. Park, and U. Sundararaj, "Impact of Foaming on the Broadband Dielectric Properties of Multi-Walled Carbon Nanotube/Polystyrene Composites," *Journal of Cellular Plastics* 50 (2014): 551–562, https://doi.org/10.1177/0021955X14539778.

54. M.-J. Jiang, Z.-M. Dang, M. Bozlar, F. Miomandre, and J. Bai, "Broad-Frequency Dielectric Behaviors in Multiwalled Carbon Nanotube/Rubber Nanocomposites," *Journal of Applied Physics* 106 (2009): 084902, https://doi.org/10.1063/1.3238306.

55. B. F. Gonçalves, P. Costa, J. Oliveira, et al., "Green Solvent Approach for Printable Large Deformation Thermoplastic Elastomer Based Piezoresistive Sensors and Their Suitability for Biomedical Applications," *Journal of Polymer Science Part B: Polymer Physics* 54 (2016): 2092–2103, https://doi.org/10.1002/polb.24118.

56. A. Kausar, "Poly(Vinylacetate)Cyanomethyl Diphenylcarbamodthioate/ Poly(Vinyl Acetate)/Carbon Black Composite-Based Sensor," *International Journal of Instrumentation Science* 5 (2016): 19–23.

57. H. Gui, X. Zhao, S. Zuo, et al., "Carbonized Syndiotactic Polystyrene/Carbon Nanotube/MXene Hybrid Aerogels With Egg-Box Structure: A Platform for Electromagnetic Interference Shielding and Solar Thermal Energy Management," *ACS Applied Materials & Interfaces* 15 (2023): 39740–39751, https://doi.org/10.1021/acsami.3c08176.

58. Y. Li, H. Wei, L. Chen, et al., "Regulating the Electronic Structure of MAX Phases Based on Rare Earth Element Sc to Enhance Electromagnetic Wave Absorption," *ACS Nano* 18 (2024): 10019–10030, https://doi.org/10.1021/acsnano.3c11585.

59. Y. Luo, H. Guo, W. Wan, P. Deng, H. Zhang, and X. Zhou, "Core–Shell Structured Fe3O4@SnO2-Reinforced Self-Healing Polyurethane Composite Films With Enhanced Electromagnetic Shielding Performance," *Journal of Materials Science* 60 (2025): 12783–12802, https://doi.org/10.1007/s10853-025-11250-5.

60. J. Wang, R. Qu, B. Ren, et al., "Lightweight, Flexible, Resilient PMIA-Based Fabric With Superior Electromagnetic Shielding Performance," *Advanced Fiber Materials* 7 (2025): 784–798, https://doi.org/10.1007/s42765-025-00520-1.

61. C. Li, S. Ma, X. Han, et al., "Malleable, Self-Healing, and Highly Thermally Conductive Interface Material Enabled by Interfacial Networks for Thermal Management," *ACS Applied Materials & Interfaces* 17 (2025): 43655–43668, https://doi.org/10.1021/acsami.5c09314.

62. K. Nath, S. Ghosh, S. K. Ghosh, P. Das, and N. C. Das, "Facile Preparation of Light-Weight Biodegradable and Electrically Conductive Polymer Based Nanocomposites for Superior Electromagnetic Interference Shielding Effectiveness," *Journal of Applied Polymer Science* 138 (2021): 50514, https://doi.org/10.1002/app.50514.

63. C. Xu, X. Huang, C. Li, Y. Chen, B. Lin, and X. Liang, "Design of "Zn^{2+} Salt-Bondings" Cross-Linked Carboxylated Styrene Butadiene Rubber With Reprocessing and Recycling Ability via Rearrangements of Ionic Cross-Linkings," *ACS Sustainable Chemical Engineering* 4 (2016): 6981–6990, https://doi.org/10.1021/acssuschemeng.6b01897.

64. V. Ugraskan, B. Isik, O. Yazici, and F. Cakar, "Comparative Physicochemical Characterization of ULTEM/SWCNT Nanocomposites: Surface, Thermal and Electrical Conductivity Analyses," *Journal of Polymer Research* 29 (2022): 254, https://doi.org/10.1007/s10965-022-03111-5.

65. J. Nayak, S. N. Choudhary, A. Pal, et al., "Synergistic Effect of MWCNT and $CoFe_2O_4$ in Ethylene-Octene Copolymer Foam for Electromagnetic Interference Shielding and Thermal Management," *Journal of Alloys and Compounds* 1038 (2025): 182718, https://doi.org/10.1016/j.jallcom.2025.182718.

66. Y.-H. Lee, C.-L. Wu, C.-W. Lai, and J.-X. Huang, "Thin, Lightweight, and Highly Efficient Electromagnetic Interference Shielding Nanocomposites Composed of a π-Conjugated Block Copolymer Nanowire/Multiwalled Carbon Nanotube Bicontinuous Interpenetrating Network," *ACS Omega* 10 (2025): 14296–14305, https://doi.org/10.1021/acsomega.5c00452.

67. A. Katheria, P. Das, J. Nayak, et al., "MXene and Fe3O4 Decorated G-C3N4 Incorporated High Flexible Hybrid Polymer Composite for Enhanced Electrical Conductivity, EMI Shielding and Thermal Conductivity," *Next Materials* 6 (2025): 100292, https://doi.org/10.1016/j.nxmate.2024.100292.

68. S. Ghosh, S. Ganguly, P. Das, et al., "Fabrication of Reduced Graphene Oxide/Silver Nanoparticles Decorated Conductive Cotton Fabric for High Performing Electromagnetic Interference Shielding and Antibacterial Application," *Fibers and Polymers* 20 (2019): 1161–1171, https://doi.org/10.1007/s12221-019-1001-7.

69. F. Qi, C. Li, Y. Jing, and F. Chen, "Precision-and-Flexibility Optimized Wearable Dual-Channel EEG Acquisition System," *Discoveries in Applied Sciences* 7 (2025): 102, https://doi.org/10.1007/s42452-025-06516-1.

70. D. Mermi Dibek and B. Baykan, "Eye Closure Sensitivity and Related EEG Findings: Persistence Rates and Classification of Epilepsy Syndromes by the International League Against Epilepsy," *Epileptic Disorders* 27 (2025): 407–419, https://doi.org/10.1002/epd2.70014.

71. X. Zhong, G. Li, C. Xu, R. Luo, J. Meng, and G. Schalk, "Detection of Eye Movements and Eye Blinks Using a Portable Two-Channel EEG Platform," *Journal of Neuroscience Methods* 425 (2026): 110616, https://doi.org/10.1016/j.jneumeth.2025.110616.

72. A. I. Triggiani, L. Liuzzi, K. Scheman, and M. Hallett, "A Brake on the Blink: EEG Antecedents of Movement Suppression and Urge to Move," *Clinical Neurophysiology* 179 (2025): 2110997, https://doi.org/10.1016/j.clinph.2025.2110997.

73. Z. Shi, B. Jiang, S. Liang, et al., "Claw-Shaped Flexible and Low-Impedance Conductive Polymer Electrodes for EEG Recordings: Anemone Dry Electrode," *Science China Technological Sciences* 66 (2023): 255–266, https://doi.org/10.1007/s11431-022-2231-3.

74. K. Motiepor, S. Bakhtiyari, A. Jahanshahi, and R. Bagherzadeh, "Stretchable Clutter-Free E-Textile EEG Cap: Advancing Seamless Wearable Solutions for Emerging Neuroimaging Applications," *Sensors and Actuators A: Physical* 387 (2025): 116454, https://doi.org/10.1016/j.sna.2025.116454.

75. G. Li, J. Wu, Y. Xia, et al., "Towards Emerging EEG Applications: A Novel Printable Flexible ag/AgCl Dry Electrode Array for Robust Recording of EEG Signals at Forehead Sites," *Journal of Neural Engineering* 17 (2020): 026001, https://doi.org/10.1088/1741-2552/ab71ea.